

Conditional diffusion models for downscaling & bias correction of Earth system model precipitation

*

Michael Aich^{1,2*}, Philipp Hess^{1,2}, Baoxiang Pan³,
Sebastian Bathiany^{1,2}, Yu Huang¹, Niklas Boers^{1,2,4}

¹Technical University Munich, Munich, Germany; School of Engineering & Design, Earth System Modelling.

²Potsdam Institute for Climate Impact Research, Potsdam, Germany.

³Institute of Atmospheric Physics, Chinese Academy of Sciences, Beijing, China.

⁴Global Systems Institute and Department of Mathematics, University of Exeter, Exeter, UK.

*Corresponding author. E-mail: michael.aich@tum.de;

Abstract

Climate change exacerbates extreme weather events like heavy rainfall and flooding. As these events cause severe losses of property and lives, accurate high-resolution simulation of precipitation is imperative. However, existing Earth System Models (ESMs) struggle with resolving small-scale dynamics and suffer from biases, especially for extreme events. Traditional statistical bias correction and downscaling methods fall short in improving spatial structure, while recent deep learning methods lack controllability over the output and suffer from unstable training. Here, we propose a novel machine learning framework for simultaneous bias correction and downscaling. We train a generative diffusion model in a supervised way purely on observational data. We map observational and ESM data to a shared embedding space, where both are unbiased towards each other and train a conditional diffusion model to reverse the mapping. Our method can be used to correct any ESM field, as the training is independent of the ESM. Our approach ensures statistical fidelity, preserves large-scale spatial patterns and outperforms existing methods especially regarding extreme events and small-scale spatial features that are crucial for impact assessments.

Keywords: precipitation simulation, statistical downscaling, bias correction, conditional diffusion models, extreme weather events, Earth system modelling

1 Introduction

With global warming, we anticipate more intense rainfall events and associated natural hazards, e.g. in terms of floods and landslides, in many regions of the world [Lee et al., 2023]. Understanding and accurately simulating precipitation is particularly important for adaptation planning and, hence, for mitigating damages and reducing risks associated with climate change. Earth System Models (ESMs) play a crucial role in simulating precipitation patterns for both historical and future scenarios. However, these simulations are computationally extremely demanding, primarily because they require solving complex partial differential equations. To manage the computational load, ESMs resort to approximate solutions on discretized grids with coarse spatial resolution (typically around 100 km). The consequence is that these models do not resolve small-scale dynamics such as many of the processes relevant to precipitation generation. This leads to considerable biases in ESM fields compared to observations. Moreover, the coarse spatial resolution prevents accurate projections of localized precipitation extremes. The precipitation fields simulated by ESMs can, therefore, not be directly used for impact assessments [Zelinka et al., 2020] and especially tasks like water resource and flood management, which demand precise spatial data at high resolution [Gutmann et al., 2014].

Statistical bias correction methods can be used as a post-processing to adjust statistical biases. Quantile mapping (QM) is the most common method for improving the statistics of ESM precipitation fields [Tong et al., 2021, Gudmundsson et al., 2012, Cannon et al., 2015]. QM reduces the bias using a mapping that, locally at each grid cell, aligns the estimated cumulative distribution of the model output with the observed precipitation patterns over a reference time period. While QM is effective in correcting distributions of single grid cells, it falls short in improving the spatial structure and patterns of precipitation simulations [Hess et al., 2022]. Visual inspection shows that ESM precipitation remains too smooth compared to observational data after applying quantile mapping (Fig. 3).

To address these problems, deep learning methods have recently been introduced [Hess et al., 2023, Pan et al., 2021, François et al., 2021, Hess et al., 2022]. In these approaches, the statistical relationships between model simulations and observational data are learned implicitly. A general constraint when using machine learning methods for bias correction is that individual samples of observational and Earth System Model data are always unpaired. A sample, in this context, is a specific weather situation at a specific point in time. The reason for this lack of pairs is that simulations, even with very similar initial conditions, diverge already after a short period of time due to the chaotic nature of the underlying atmospheric dynamics. Currently, one can, therefore, not utilize the wide range of supervised ML techniques that have shown great success in various disciplines in recent years and the available options are consequently restricted to self- and unsupervised machine learning methods. Recent studies [Hess et al., 2023, Pan et al., 2021, François et al., 2021, Hess et al., 2022] applied generative adversarial networks (GANs [Goodfellow et al., 2020]) and specifically cycleGANs [Zhu et al., 2017] to improve upon existing bias correction techniques. A major limitation of GAN-based approaches is that stability and convergence of the

training process are hard to control and that it is challenging to find metrics that indicate training convergence. Also, GANs often suffer from mode collapse, where only a part of the target probability distribution is approximated by the GAN.

As noted above, the low spatial resolution of ESM fields prevents local risk and impact assessment, which necessitates the additional use of downscaling methods. In line with the climate literature, we refer to increasing the spatial resolution as downscaling throughout our manuscript, although we are aware that, especially in the machine learning literature, the term upsampling is more prevalent. We use the term downscaling only when we want to increase the information content in an image as well as the number of pixels. When we refer to upsampling (downsampling), we only mean an increase (decrease) in the number of pixels. Statistical downscaling aims to learn a transformation from the low resolution ESM fields to high resolution observations. Recent developments lean towards using machine learning methods for this task [Rampal et al., 2022, Hobeichi et al., 2023]. The potential for machine learning based downscaling methods was shown already in [Vandal et al., 2017]. The work presented a downscaling approach built on purely convolutional networks. More recent work [Wan et al., 2024] introduced a framework for downscaling and bias correction, combining a diffusion model for downscaling and a model based on optimal transport for bias correction [Cuturi, 2013]. Optimal transport learns a map between two data distributions in an unsupervised setting. The downside of their framework is its computational expense. The effectiveness also has not been demonstrated on real observational and ESM fields yet.

Diffusion models (DMs) have recently emerged as the state-of-the-art ML approach for conditional image generation [Saharia et al., 2022b, Rombach et al., 2022, Saharia et al., 2022c] and image-to-image translation [Saharia et al., 2022a], mostly outperforming GANs across different tasks. Diffusion models (Fig. 1 and S1) avoid the common issues present with GANs in exchange for slower speed at inference. A diffusion model consists of a forward and a backward process. During the forward process, noise is added to an image in subsequent steps to gradually remove its content. The amount of noise added follows a predefined equation. During the backward process, a neural network is trained to reverse each of these individual noising steps to recover the original image. The trained diffusion model can generate an image of the training data distribution, given a noise image as input.

We present here a framework based on state-of-the-art diffusion models that allows to perform both bias correction and downscaling with one single network. This network can, in principle, be any supervised machine learning method. We use a single conditional diffusion model (Fig. 1 and Fig. S1) to correct low resolution (LR) ESM fields towards high resolution (HR) observational data (OBS). In general, our task of bias correction and downscaling can be seen as taking a field from a distribution $p(ESM)$ and transforming it into a field from a conditional distribution $p(OBS|ESM)$. We cannot directly learn such a downscaling and bias correction transformation because ESM and OBS are unpaired. Our framework, therefore, introduces transformations f and g that map ESM and OBS data to a shared embedding space (see Methods and Fig. 1A). On this shared embedding space, we can train a conditional diffusion model

to approximate the inverse of f . We are then able to bias correct and downscale ESM fields by first mapping them to the shared embedding space and then projecting them to the OBS dataset with the trained diffusion model (Fig. 1B and Fig. 1C). This framework offers great flexibility as it can be applied to any ESM.

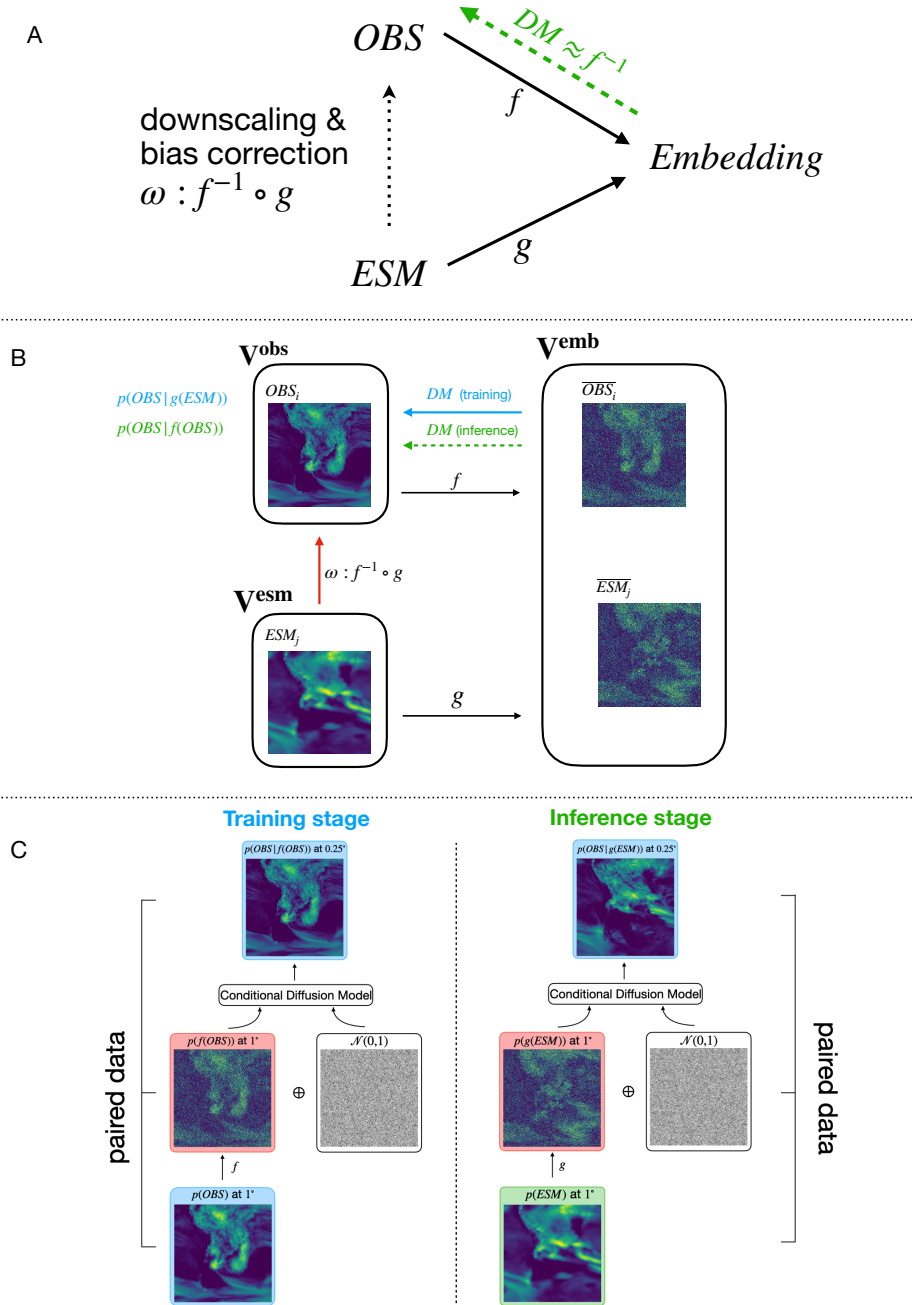


Fig. 1 (A) Schematic overview of our approach. Bias correction and downscaling can be formulated as a mapping ω from the ESM data space to the data space of observations (OBS) used for training. We first map both datasets to a shared embedding space and then learn the inverse of the mapping f with a diffusion model DM . We achieve a correction of the ESM data by applying $DM \circ g$. (B) Our framework allows to train a single model for bias correction and downscaling in a supervised way despite the unpaired nature of observations (OBS) and Earth system model (ESM) fields. We construct functions f, g that map $OBS \in \mathbf{V}^{obs}$ and $ESM \in \mathbf{V}^{esm}$ fields to a shared embedding space \mathbf{V}^{emb} . By inverting f , we can rewrite ω as $\omega = f^{-1} \circ g$. We learn the inverse f^{-1} with a conditional diffusion model DM . This model is trained (blue arrow) on pairs to approximate the map from $f(OBS)$ to OBS (see Methods for details). Because $f(OBS)$ and $g(ESM)$ share the embedding space (and are identically distributed by construction), we can evaluate (green arrow) the conditional diffusion model DM on the embedded ESM data $g(ESM)$ and thereby approximate the bias correction and downscaling function $\omega = f^{-1} \circ g \approx DM \circ g$. (C) Left: Training process of the conditional diffusion model $DM \approx f^{-1}$. Note that the individual samples of the input OBS and their embeddings $f(OBS)$, as well as the embeddings $f(OBS)$ and the output of $DM \approx f^{-1}$ are paired, respectively. Right: Inference process of $DM \approx f^{-1}$. In this case, the individual samples of the input ESM , their embeddings $g(ESM)$, and the output of $DM \approx f^{-1}$ are paired, respectively. It is not necessary for the training embedding samples to be paired with the inference embedding samples. See Fig. S1 for details.

2 Results

The ability of the diffusion model DM to approximate f^{-1} and the effectiveness of the transformations f, g will determine the overall performance of the downscaling and bias correction model $\omega = DM \circ g$. Therefore, we first investigate the effectiveness of the embedding transformations f and g , followed by an analysis of the downscaling and bias correction performance of the diffusion model DM , on the observational dataset. Once we have shown that both work as expected, we investigate the performance of the diffusion model in bias correction and downscaling of the ESM precipitation fields. Without loss of generality, we chose the 0.25° ERA5 reanalysis [Hersbach et al., 2020] data as observational data and the state-of-the-art GFDL-ESM4 [Dunne et al., 2020] at 1° as our ESM.

2.1 Embedding evaluation

The transformations f, g are chosen such that they map the observational (OBS) and model (ESM) data to a common embedding space \mathbf{V}^{emb} , where all samples are identically distributed. For constructing f and g we need $f(ERA5)$ and $g(GFDL)$ to be unbiased with respect to each other. The transformations need to be chosen such that the embedded data share the same distribution and the same power spectral density (PSD). We assess if they are statistically unbiased towards each other by analyzing their histograms latitude / longitude profiles, as well as their spatial spectra. Figure S2 shows that $f(ERA5)$ and $g(GFDL)$ have the same spatial distribution (Fig. S2A) with minor differences in temporal statistics shown by the histogram (Fig. S2B) and latitudinal/ longitudinal profiles (Fig. S2C and Fig. S2D).

The individual operations that make up the transformations f and g do not change the large-scale patterns of their respective inputs, as desired for a valid bias correction. The goal of the downscaling and bias correction ω (Fig. 1) is to rely on the unbiased large-scale patterns of the ESM and correct statistics, as well as small-scale patterns. The transformation g conserves the unbiased information from the ESM by construction. Therefore, we want the diffusion model, approximating f^{-1} , to also preserve unbiased information.

The extreme case of erasing all detail with large amounts of noise leads to learning the unconditional distribution $p(ERA5)$, which is then not a correction of $GFDL$ but a generative emulation of the ERA5 reanalysis data. We test this by adding the same amount of noise to the output of our diffusion model that was added to create $g(GFDL)$. This ensures that both the downscaled and bias corrected fields, as well as the original GFDL fields, lack the small-scale details up to the same point.

To verify that large-scale patterns are preserved by the diffusion model, we compute image similarity metrics between the low pass filtered version of the input of the diffusion model (embedded ERA5 data $f(ERA5)$) and the low pass filtered output of the diffusion model $DM(f(ERA5))$. The output of the low pass filter leaves the large-scale features unchanged. The comparison yields an average structural similarity index (SSIM [Wang et al., 2004]) value of 0.8 and a Pearson correlation coefficient of

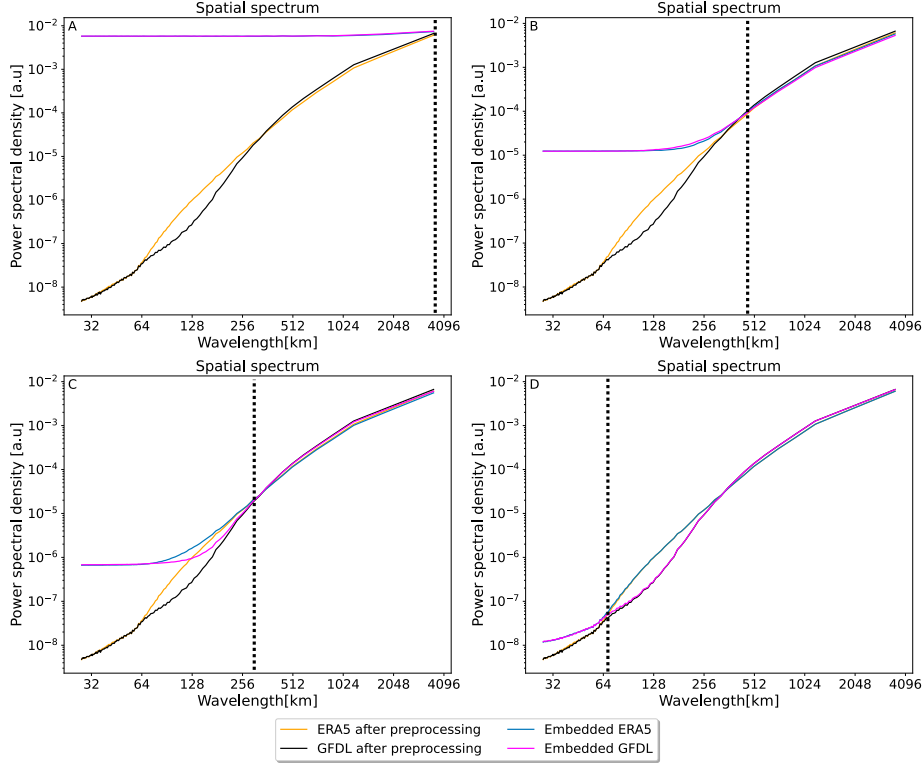


Fig. 2 Power spectral densities (PSDs) for different choices of the noise scale of the diffusion model. The noise scale s (dashed line) is a hyperparameter that can be chosen depending on the ESM and observational datasets, as well as on the specific task. For the maximal choice of s (**A**) all information in the observations (ERA5) and model simulations (GFDL) is noised and thereby destroyed. Conditioning on pure noise makes the task equivalent to unconditional image generation. The diffusion model will learn to generate observational fields with no relation to the ESM fields. When s is chosen to be minimal, there will be no noising and the conditional generation will directly replicate the condition, i.e. the ESM field. In (**B**) we chose s as the point where the PSDs of the observational and simulated datasets intersect. We then apply sufficiently many forward diffusion noising steps to both datasets, destroying small-scale structure until they agree in the PSD. We call scales smaller than s small scales and scales larger than s large scales. In (**C**) and (**D**), the effects of choosing a smaller noise scale s are shown. Prior knowledge about the ESM or its accuracy can also guide the choice of s .

0.9 for the validation dataset. This verifies that large-scale patterns are well preserved by the diffusion model.

Our diffusion model is able to reconstruct high-resolution fields following the ERA5 distribution from embedded ERA5 fields $f(ERA5)$, with only minor discrepancies in

small-scale patterns (Fig. S2A). A comparison between the mean absolute spatial-temporal difference between GFDL and ERA5 fields yields a bias of 0.3 mm/d. The downscaling and bias correction of our diffusion model reduces this bias to 0.1 mm/d. Our diffusion model thus approximates f^{-1} well and we successfully created a shared embedding space in which $f(ERA5)$ and $g(GFDL)$ are identically distributed.

2.2 Evaluation of downscaling and bias correction performance

We investigate the inference performance of our diffusion model on embedded GFDL data $g(GFDL)$. We compare the downscaling and bias correction performance of our diffusion model to a benchmark consisting of first applying bi-linear upsampling followed by QM for bias correction.

Figure 3 allows for a qualitative comparison between the different individual precipitation fields. The upsampled *GFDL* fields, as well as our benchmark consisting of the upsampled and QM-corrected *GFDL* fields, are visually too smooth. They therefore appear blurry compared to the ERA5 precipitation fields despite being on the same spatial resolution of 0.25° . Our diffusion model produces detailed, high resolution outputs that are visually indistinguishable from the *ERA5* reanalysis that we treat as ground truth.

A comparison between the absolute temporally and absolute spatial-temporally averaged diffusion model-corrected GFDL and ERA5 fields (Fig. 4A) yields a bias of 0.29 mm/d. This is a significant improvement over the original GFDL dataset which yields a bias of 0.69 mm/d (Fig. 4B). Our diffusion model performs on par with the state-of-the-art bias correction performance of our benchmark that is by design optimal for this task, at 0.26 mm/d (Fig. 4D).

There are large differences between GFDL and ERA5 data in small-scale patterns (Fig. 5A). The histogram of precipitation intensities (Fig. 5B) also confirms that the ESM is only really accurate for precipitation events up to 40 mm/d, after which the respective frequencies diverge. The latitudinal and longitudinal mean profiles (Fig. 5C and Fig. 5D) indicate the presence of regional biases.

Our framework demonstrates comparable skill to the QM-based benchmark in correcting the latitude and longitude profiles, for which QM is near optimal by construction (Fig. 5C and Fig. 5D). Comparing the histograms (Fig. 5B and Fig. S3) shows a similar performance of our diffusion model compared to the benchmark while even slightly outperforming it for extreme values.

For the spatial patterns and especially the small-scale spatial features, the QM benchmark shows only slight improvements over the original GFDL data (Fig. 5A). The diffusion model is vastly superior in correcting these small-scale spatial patterns (Fig. 5A and Fig. 3) and almost completely removes the small-scale biases, as seen in the spatial PSD.

Our method hence accurately preserves the large-scale precipitation content, while successfully correcting small-scale structure of the precipitation fields, as well as statistical biases in terms of histograms and latitude / longitude profiles (Fig. 5).

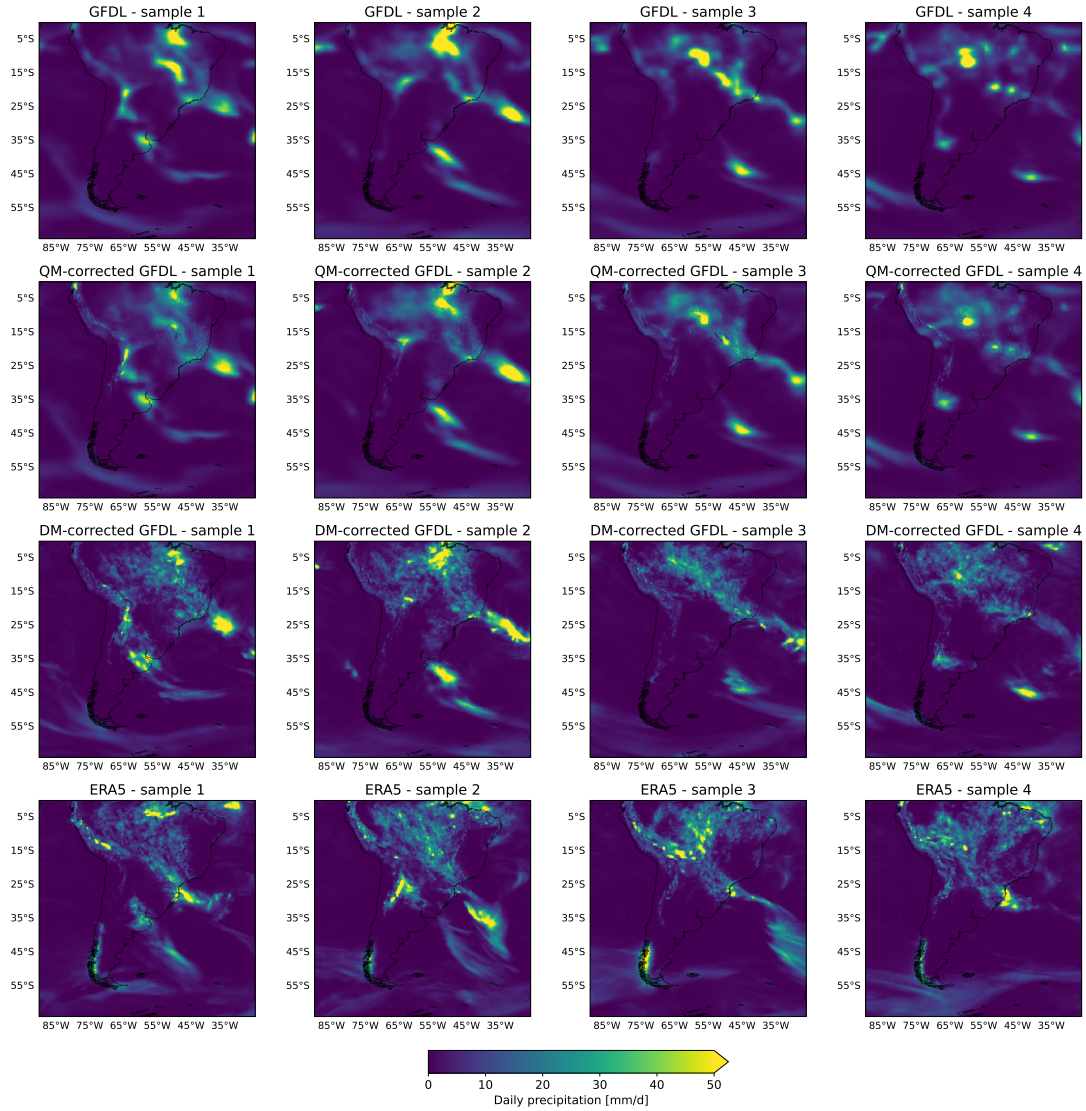


Fig. 3 Comparative visualization of individual randomly selected samples: Each row presents four samples of the same dataset. The top row shows GFDL ESM4 data, bi-linearly upsampled to 0.25° to match the other fields. The second row shows QM-corrected and the third row diffusion model-corrected GFDL fields. The bottom row shows samples of the original ERA5 data, which are unpaired to the GFDL fields above. Visual inspection shows that the diffusion model correction greatly improves upon the QM correction in terms of producing realistic spatial patterns, since the QM-corrected fields remain way too blurry compared to the HR ERA5 data. There is no visual difference between the details and sharpness of diffusion model-corrected GFDL fields compared to ERA5.

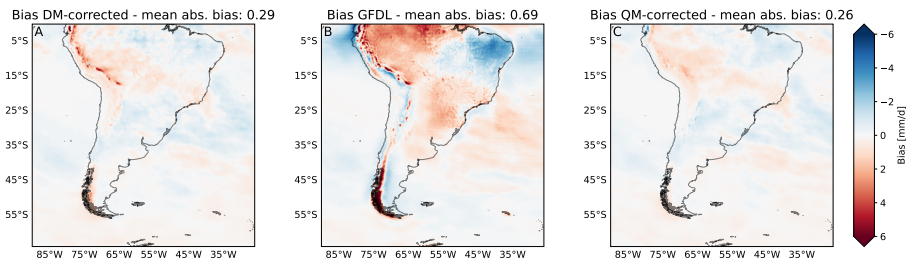


Fig. 4 Bias of the GFDL ESM4 model and the QM- and diffusion model-corrections, defined as the difference between long-term temporal averages of all validation samples. Specifically, the temporally averaged bias fields with respect to ERA5 are shown for **(A)** the diffusion model correction, **(B)** the uncorrected GFDL and **(C)** the QM correction. Results indicate a substantial improvement of our diffusion model (A) and the benchmark (C) over just upsampling GFDL to 0.25° . The absolute bias on top of each panel is given by the mean absolute value of the differences over the spatial and temporal dimension with respect to ERA5.

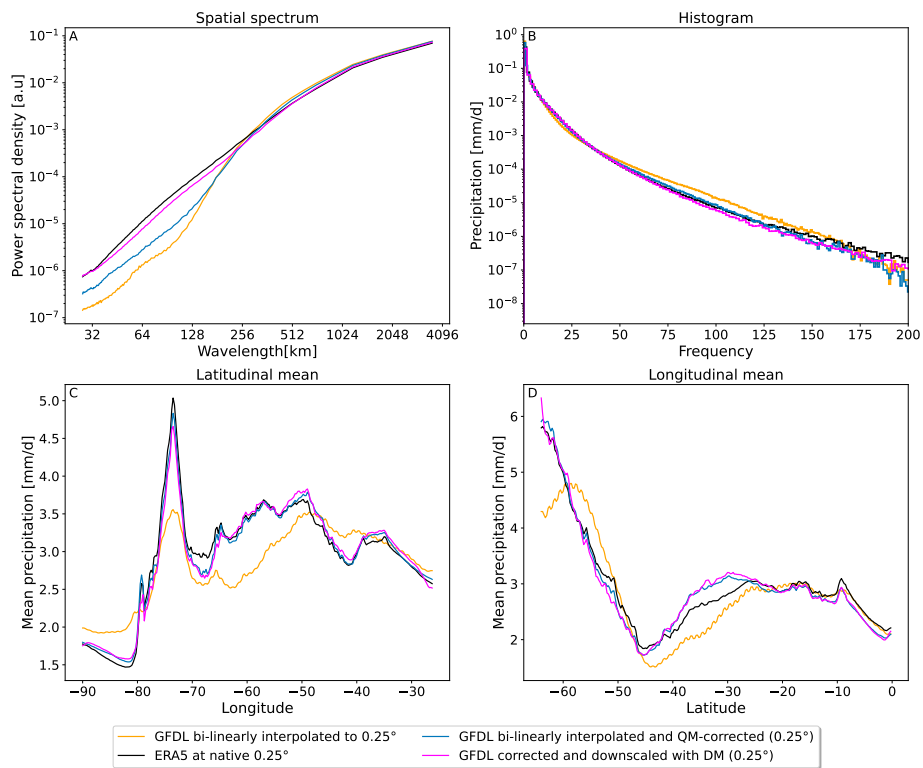


Fig. 5 Comparison of GFDL (bi-linearly upsampled to 0.25°) (orange) and ERA5 (black) to diffusion model-corrected GFDL (magenta) and QM-corrected GFDL fields (blue) as our benchmark. The Power spectral density (PSD) plot (**A**) shows that the diffusion model corrects the small-scale spatial details far better than our benchmark. The spectrum aligns very well with the high resolution ERA5 target data. The histograms (**B**) as well as the latitude (**C**) and longitude (**D**) profiles show substantial improvements compared to the uncorrected GFDL data.

3 Discussion

We introduced a framework based on generative machine learning that enables to do both bias correction and downscaling of Earth system model fields with a single diffusion model. We achieve this by first mapping observational fields and ESM data to a shared embedding space and then applying the learned inverse of the observation embedding transformation to the embedded ESM fields. We learn the inverse transformation with a conditional diffusion model. Although the underlying observational and ESM fields are unpaired, our framework allows for training on paired data, and therefore any supervised machine learning method can be adopted to the task, which allows for more flexibility. The diffusion model is trained on individual samples and has successfully learned to reproduce the statistics of observational data. For the observational ground truth, we chose the ERA5 reanalysis, and for the ESM data to be corrected and downscaled, we chose fields from GFDL-ESM4.

Our diffusion model corrects small-scale biases of the ESM fields, while completely preserving the large-scale structures, which is key for impact assessments, especially with regard to extremes and local impacts in terms of floods or landslides. The diffusion model performs particularly well for extreme events where traditional methods struggle. The method improves the temporal precipitation distribution at a grid cell level and surpasses the state-of-the-art approach (quantile mapping) at correcting spatial patterns. The downscaling performance has also been shown to be excellent. The diffusion model manages to generate small-scale details for the low resolution ESM data, that match those of high resolution observations.

Our method is not specific to ERA5 and GFDL, because the training of the diffusion model does not directly depend on the ESM choice. A specific ESM choice will only modify a hyperparameter in the embedding transformations f and g . This, however, requires almost no fine-tuning, as the temporal frequencies can always be matched with quantile mapping. The only parameter that might change for different datasets and use cases is the amount of noise that is added to the observational and ESM datasets. We choose the amount of noise such that the PSDs of the observational ground truth and the ESM fields align beyond a certain scale. This means that we have complete flexibility in deciding which patterns we want to preserve and which we want to correct. This is a major advantage over existing GAN based approaches.

We can decrease the level of detail that is preserved by the diffusion model through increasing the amount of noise added in the transformations f and g . This leads to higher uncertainties and therefore increased variance in the outputs of the diffusion model. It is, however, not guaranteed that this increase in variance corresponds to the uncertainties of the ESM. The amount of noise added is directly proportional to the freedom the diffusion model has in generating diverse outputs and inversely proportional to the models' ability to preserve large-scale patterns.

The downscaled and bias corrected fields will automatically inherit time consistency between different samples up to the noising scale. This means that ESM fields showing two successive days will still look like two successive days after the correction.

We focused on precipitation data over the South American continent, because of its heavily tailed distribution and the pronounced spatial intermittency. Especially at small scales, precipitation data is extremely challenging to model and therefore serves as a reasonable choice to show the frameworks capabilities in a particularly difficult setting. Regional data is chosen due to computational constraints, yet the diverse terrain of our study region, encompassing land, sea, and a wide range of altitudes, enables robust testing of the downscaling and bias correction performance, also given the significant biases of the GFDL model in this region. The extension to global scales is straightforward and requires no changes in the architecture. We intend to include more variables in a consistent manner and on a global scale in future research. Optimizing the inference strategy, with speedup techniques like distillation [Luhman and Luhman, 2021], to decrease the sampling time will prove helpful in this context. Taking the growing number of diffusion model variants into consideration, a comparison between different approaches can help establish the best method suited for the general task of bias correcting and downscaling ESM fields.

It is straightforward to extend our methodology to the downscaling and bias correction of numerical or data driven weather predictions on short to medium-range or even seasonal temporal-scales. This would not require any fundamental changes in the architecture. One would, however, require a target dataset with sufficiently high resolution. The ability of the diffusion model to not disturb temporal consistency between samples can be useful in this scenario.

Declarations

Funding

Funded under the Excellence Strategy of the Federal Government and the Länder through the TUM Innovation Network EarthCare. This is ClimTip contribution #X; the ClimTip project has received funding from the European Union's Horizon Europe research and innovation programme under grant agreement No. 101137601. PH, SB, and NB acknowledge funding by the Volkswagen Foundation. BP acknowledges funding by the National Key R&D Program of China (2021YFA0718000). YH acknowledges Alexander von Humboldt Foundation for the Humboldt Research Fellowship.

Data Availability

The ERA5 reanalysis data is available for download at the Copernicus Climate Change Service (<https://cds.climate.copernicus.eu/cdsapp#!/dataset/reanalysis-era5-single-levels?tab=overview>). The CMIP6 GFDL-ESM4 is available at <https://esgf-data.dkrz.de/search/cmip6-dkrz/>.

Code Availability

The code will be made available on GitHub.

Competing interests

The authors declare no competing interests.

Ethics approval and consent to participate

Not applicable

Consent for publication

Not applicable

4 Methods

4.1 Data

For the study region, we focus on the South American continent and the surrounding oceans. Specifically, the targeted area spans from latitude 0°N to 63°S and from longitude -90°W to -27°E . The training period comprises ERA5 data from 1992-01-01 to 2011-01-01. The range of years included for evaluation on ERA5 and GFDL spans from 2011-01-02 to 2014-12-01.

ERA5

ERA5 [Hersbach et al., 2020] is a state-of-the-art atmospheric reanalysis dataset provided by the European Center for Medium-Range Weather Forecasting (ECMWF). Reanalysis refers to the process of combining observations from various sources, such as weather stations, satellites, and other instruments, with a numerical weather model to create a continuous and comprehensive representation of the Earth’s atmosphere. We use the daily total precipitation data at 0.25° horizontal resolution as the target for the diffusion model.

GFDL

The climate model output is taken from a state-of-the-art ESM from Phase 6 of the Coupled Model Intercomparison Project (CMIP6), namely the GFDL-ESM4 [Dunne et al., 2020]. The dataset contains daily precipitation data of the first ensemble member (r1i1p1f1) of the historical simulation (esm-hist). The data is available from 1850 to 2014, at 1° latitudinal and 1.25° longitudinal resolution and daily temporal resolution.

Benchmark dataset

In order to benchmark our method, we first apply bi-linear interpolation to increase the resolution of the GFDL fields from 1° to 0.25° . After that, we apply Quantile delta mapping [Cannon et al., 2015] to fit the upsampled GFDL data to the original 0.25° ERA5 data. QM is fitted on past observations, and can then be used to correct the statistics of any (past/present) ESM field towards that reference period. We use quantile delta mapping and chose the training period of ERA5 from 1992-01-01 to 2011-01-01 as the reference period for fitting GFDL to ERA5. The benchmark dataset to evaluate our approach is then constructed by applying QM to the validation period of GFDL (2011-01-02 to 2014-12-31).

Data pre-processing

The units of the GFDL data are $\text{kg m}^{-2}\text{s}^{-1}$, and for ERA5 m/h . For consistency, both are transformed to mm/d .

Our pre-processing pipeline consists of:

- only GFDL: rescaling the original $1^\circ \times 1.25^\circ$ GFDL data to $1^\circ \times 1^\circ$ (64×64 pixel).
- Add +1 mm/d precipitation to each value in order to be able to apply a log-transformation to the data.
- Apply the logarithm with base 10 in order to compress the range of values.
- Standardize the data, i.e. subtract the mean and divide by the standard deviation to facilitate training convergence.
- Transform the data to the range $[-1,1]$ in order to facilitate training convergence.

As part of the transformation g , the 1° GFDL data is bi-linearly upsampled. This and the downsampling and upsampling of ERA5 data, which is part of f , are already done during pre-processing. The downsampling of 0.25° ERA5 data (256×256 pixel) to 1° (64×64 pixel) is done by only keeping every fourth pixel in each field. For the just mentioned upsampling, we apply bi-linear interpolation to increase the resolution from 1° to 0.25° . Note that bi-linear interpolation to 0.25° does not increase the amount of information in the images compared to the 1° fields. After pre-processing the data as described, the embedding transformation f is applied. The diffusion model is trained with the pre-processed $f(ERA5)$ as a condition and the original 0.25° ERA5 data as a target. Before we apply the embedding transformation g we first pre-process the 1° GFDL data by applying quantile delta mapping (QDM [Cannon et al., 2015]) with 500 quantiles. Bi-linear upsampling is afterward used to increase the resolution to $0.25 \times 0.25^\circ$ (256×256 pixels). The pre-processed data is used as input to the embedding transformation g . The corresponding output serves as the condition during the inference process of the diffusion model.

4.2 Embedding framework

Our framework introduces transformations f & g that map OBS and ESM data to a shared embedding space $f : \mathbf{V}^{\text{obs}} \rightarrow \mathbf{V}^{\text{emb}}$ and $g : \mathbf{V}^{\text{esm}} \rightarrow \mathbf{V}^{\text{emb}}$. The goal is to do bias correction and downscaling of ESM fields, i.e., to obtain samples from the conditional distribution $\omega = p(OBS|ESM)$. Training a conditional model to approximate this distribution directly is not possible because OBS and ESM are unpaired. The arrows in the diagram of Figure 1 show that we can represent the mapping that achieves the bias correction and downscaling as $\omega = f^{-1} \circ g$. Our idea is to approximate f^{-1} with a neural network $f^{-1} \approx \epsilon$. We chose a conditional diffusion model (DM), denoted by the conditional distribution $p(OBS|f(OBS))$, to approximate $f^{-1} = DM : \mathbf{V}^{\text{emb}} \rightarrow \mathbf{V}^{\text{obs}}$. The diffusion model (Fig. 1C) is only trained on pairs $(OBS, f(OBS))$. The shared embedding space allows us to evaluate the trained model on ESM embeddings $p(OBS|g(ESM))$, as all embeddings are identically distributed.

4.2.1 Constructing the embedding space

The goal of f and g is to map OBS and ESM to a shared embedding space, where $f(OBS)$ and $g(ESM)$ are identically distributed (Fig. 1). To achieve this, both embedded datasets need to be unbiased towards each other. OBS and ESM are biased towards each other in terms of statistical biases between the distributions and biases

between small-scale patterns visible in the spatial power spectral density (PSD) (Fig S2A).

As mentioned earlier, the input to the embedding transformation f is 0.25° ERA5 data, which is first downsampled, then upsampled and pre-processed. The input to the embedding transformation g is the upsampled and pre-processed 0.25° GFDL data. By first downsampling ERA5 to 1° and then upsampling it to 0.25° we ensure that the fields match the information content of the original 1° GFDL fields.

To remove the small-scale pattern bias, we apply a noising procedure analogous to the forward diffusion process as part of f and g . Both ERA5 and GFDL data are noised up to a certain spatial scale in the PSD, denoted by the point s . The scale s is determined by the point where ERA5 and GFDL start to disagree in the PSD (Fig. 2), i.e., the intersection between the two. Adding noise ensures that $f(ERA5)$ is unbiased compared to $g(GFDL)$ in the PSD by erases all information beneath s . The transformations f and g utilize the same cosine scheduler as the forward diffusion process to add Gaussian noise to the data. ERA5 data undergoes 50 noise steps within f , while g applies the same 50 noise steps to the GFDL data.

We ensure the observational and ESM data have aligned distributions by incorporating Quantile Mapping (QM) directly into the transformation g . It can directly be applied in pre-processing and only needs to be included in g . It’s important to clarify that QM is not included because the diffusion model is unable to do bias correction. QM is only used as a tool in our framework to ensure that in the embedding space $f(ERA5)$ and $g(GFDL)$ are identically distributed, such that $g(GFDL)$ can be used for the inference of the diffusion model.

4.2.2 Determining the noising scale

The choice of the spatial scale s influences up to which scale we correct the spatial PSD. We note that the PSD shows spectral distributions normalized to 1; therefore, we can still observe slight changes above s when small-scale patterns are corrected. The point s is a hyperparameter chosen before training and purely depends on the datasets ESM and OBS and can be adjusted to the specific needs in a given context and task.

In the extreme case, where s is maximal, the conditional images will contain pure noise (Fig. 2A). In this case, the diffusion model is equivalent to an unconditional model. As an unconditional model, the diffusion model will correct all biases at all spatial scales, however, at the expense of completely losing any paring between the condition and the output. We chose s to be at the intersection of the ERA5 and GFDL spectrum around 512 km (Fig. 2B). Thereby, we trust in the ESM’s ability to model large-scale structures above the point s , which we do not want to correct with the diffusion model.

4.3 Network architecture and training

The general architecture of our diffusion model DM consists of a Denoising Diffusion Probabilistic Model (DDPM) architecture [Ho et al., 2020] conditioned on low-resolution images. This is similar to a single block of a cascading super-resolution

model. We employ current state-of-the-art techniques to facilitate faster convergence and find the following to be important for convergence and sample quality [Saharia et al., 2022b]: The memory efficient architecture, "Efficient U-Net", in combination with dynamic clipping and noise conditioning augmentation [Ho et al., 2022] turned out to be effective for our relatively small dataset. We adopt the Min-SNR [Hang et al., 2023] formulation to weight the loss terms of different timesteps based on the clamped signal-to-noise ratios. The diffusion model architecture utilizes a cosine schedule for noising the target data and a linear schedule for the condition during noise condition augmentation with 1000 steps each. The diffusion model is trained to do v-prediction instead of noise prediction. The U-Net follows the $64 \times 64 \rightarrow 256 \times 256$ Efficient U-Net architecture ([Saharia et al., 2022b]). The diffusion model is trained for 80 epochs using the ADAM optimizer [Kingma and Ba, 2014] with a batch size of 4 and a learning rate of $1e^{-4}$.

References

- [Cannon et al., 2015] Cannon, A. J., Sobie, S. R., and Murdock, T. Q. (2015). Bias correction of gcm precipitation by quantile mapping: how well do methods preserve changes in quantiles and extremes? *Journal of Climate*, 28(17):6938–6959.
- [Cuturi, 2013] Cuturi, M. (2013). Sinkhorn distances: Lightspeed computation of optimal transport. *Advances in neural information processing systems*, 26.
- [Dunne et al., 2020] Dunne, J. P., Horowitz, L. W., Adcroft, A. J., Ginoux, P., Held, I. M., John, J. G., Krasting, J. P., Malyshev, S., Naik, V., Paulot, F., Shevliakova, E., Stock, C. A., Zadeh, N., Balaji, V., Blanton, C., Dunne, K. A., Dupuis, C., Durachta, J., Dussin, R., Gauthier, P. P. G., Griffies, S. M., Guo, H., Hallberg, R. W., Harrison, M., He, J., Hurlin, W., McHugh, C., Menzel, R., Milly, P. C. D., Nikonov, S., Paynter, D. J., Ploshay, J., Radhakrishnan, A., Rand, K., Reichl, B. G., Robinson, T., Schwarzkopf, D. M., Sentman, L. T., Underwood, S., Vahlenkamp, H., Winton, M., Wittenberg, A. T., Wyman, B., Zeng, Y., and Zhao, M. (2020). The GFDL Earth System Model Version 4.1 (GFDL-ESM 4.1): Overall Coupled Model Description and Simulation Characteristics. *Journal of Advances in Modeling Earth Systems*, 12(11):e2019MS002015. eprint: <https://onlinelibrary.wiley.com/doi/pdf/10.1029/2019MS002015>.
- [François et al., 2021] François, B., Thao, S., and Vrac, M. (2021). Adjusting spatial dependence of climate model outputs with cycle-consistent adversarial networks. *Climate dynamics*, 57:3323–3353.
- [Goodfellow et al., 2020] Goodfellow, I., Pouget-Abadie, J., Mirza, M., Xu, B., Warde-Farley, D., Ozair, S., Courville, A., and Bengio, Y. (2020). Generative adversarial networks. *Communications of the ACM*, 63(11):139–144.
- [Gudmundsson et al., 2012] Gudmundsson, L., Bremnes, J. B., Haugen, J. E., and Engen-Skaugen, T. (2012). Downscaling rcm precipitation to the station scale using statistical transformations—a comparison of methods. *Hydrology and Earth System Sciences*, 16(9):3383–3390.
- [Gutmann et al., 2014] Gutmann, E., Pruitt, T., Clark, M. P., Brekke, L., Arnold, J. R., Raff, D. A., and Rasmussen, R. M. (2014). An intercomparison of statistical downscaling methods used for water resource assessments in the u nited s tates. *Water Resources Research*, 50(9):7167–7186.
- [Hang et al., 2023] Hang, T., Gu, S., Li, C., Bao, J., Chen, D., Hu, H., Geng, X., and Guo, B. (2023). Efficient diffusion training via min-snr weighting strategy. In *Proceedings of the IEEE/CVF International Conference on Computer Vision*, pages 7441–7451.
- [Hersbach et al., 2020] Hersbach, H., Bell, B., Berrisford, P., Hirahara, S., Horányi, A., Muñoz-Sabater, J., Nicolas, J., Peubey, C., Radu, R., Schepers, D., Simmons, A., Soci, C., Abdalla, S., Abellan, X., Balsamo, G., Bechtold, P., Biavati, G., Bidlot, J., Bonavita, M., De Chiara, G., Dahlgren, P., Dee, D., Diamantakis, M., Dragani, R., Flemming, J., Forbes, R., Fuentes, M., Geer, A., Haimberger, L., Healy, S., Hogan, R. J., Hólm, E., Janisková, M., Keeley, S., Laloyaux, P., Lopez, P., Lupu, C., Radnoti, G., de Rosnay, P., Rozum, I., Vamborg, F., Villaume, S., and Thépaut, J.-N. (2020). The ERA5 global reanalysis. *Quarterly Journal of the Royal Meteorological Society*, 146(730):1999–2049. eprint:

<https://onlinelibrary.wiley.com/doi/pdf/10.1002/qj.3803>.

- [Hess et al., 2022] Hess, P., Driike, M., Petri, S., Strnad, F. M., and Boers, N. (2022). Physically constrained generative adversarial networks for improving precipitation fields from earth system models. *Nature Machine Intelligence*, 4(10):828–839.
- [Hess et al., 2023] Hess, P., Lange, S., Schötz, C., and Boers, N. (2023). Deep learning for bias-correcting cmip6-class earth system models. *Earth’s Future*, 11(10):e2023EF004002.
- [Ho et al., 2020] Ho, J., Jain, A., and Abbeel, P. (2020). Denoising diffusion probabilistic models. *Advances in neural information processing systems*, 33:6840–6851.
- [Ho et al., 2022] Ho, J., Saharia, C., Chan, W., Fleet, D. J., Norouzi, M., and Salimans, T. (2022). Cascaded diffusion models for high fidelity image generation. *Journal of Machine Learning Research*, 23(47):1–33.
- [Hobeichi et al., 2023] Hobeichi, S., Nishant, N., Shao, Y., Abramowitz, G., Pitman, A., Sherwood, S., Bishop, C., and Green, S. (2023). Using machine learning to cut the cost of dynamical downscaling. *Earth’s Future*, 11(3):e2022EF003291.
- [Kingma and Ba, 2014] Kingma, D. P. and Ba, J. (2014). Adam: A method for stochastic optimization. *arXiv preprint arXiv:1412.6980*.
- [Lee et al., 2023] Lee, H., Calvin, K., Dasgupta, D., Krinner, G., Mukherji, A., Thorne, P., Trisos, C., Romero, J., Aldunce, P., Barret, K., Blanco, G., Cheung, W. W., Connors, S. L., Denton, F., Diongue-Niang, A., Dodman, D., Garschagen, M., Geden, O., Hayward, B., Jones, C., Jotzo, F., Krug, T., Lasco, R., Lee, Y.-Y., Masson-Delmotte, V., Meinshausen, M., Mintenbeck, K., Mokssit, A., Otto, F. E., Pathak, M., Pirani, A., Poloczanska, E., Pörtner, H.-O., Revi, A., Roberts, D. C., Roy, J., Ruane, A. C., Skea, J., Shukla, P. R., Slade, R., Slangen, A., Sokona, Y., Sörensson, A. A., Tignor, M., van Vuuren, D., Wei, Y.-M., Winkler, H., Zhai, P., Zommers, Z., Hourcade, J.-C., Johnson, F. X., Pachauri, S., Simpson, N. P., Singh, C., Thomas, A., Totin, E., Arias, P., Bustamante, M., Elgizouli, I., Flato, G., Howden, M., Méndez-Vallejo, C., Pereira, J. J., Pichs-Madruga, R., Rose, S. K., Saheb, Y., Rodríguez, R. S., Urge-Vorsatz, D., Xiao, C., Yassaa, N., Alegría, A., Armour, K., Bednar-Friedl, B., Blok, K., Cissé, G., Dentener, F., Eriksen, S., Fischer, E., Garner, G., Guivarch, C., Haasnoot, M., Hansen, G., Hauser, M., Hawkins, E., Hermans, T., Kopp, R., Leprince-Ringuet, N., Lewis, J., Ley, D., Ludden, C., Niamir, L., Nicholls, Z., Some, S., Szopa, S., Trewin, B., van der Wijst, K.-I., Winter, G., Witting, M., Birt, A., Ha, M., Romero, J., Kim, J., Haites, E. F., Jung, Y., Stavins, R., Birt, A., Ha, M., Orendain, D. J. A., Ignon, L., Park, S., and Park, Y. (2023). Ipcc, 2023: Climate change 2023: Synthesis report, summary for policy-makers. contribution of working groups i, ii and iii to the sixth assessment report of the intergovernmental panel on climate change [core writing team, h. lee and j. romero (eds.)]. ipcc, geneva, switzerland. Technical Report 10.59327/IPCC/AR6-9789291691647.001, Intergovernmental Panel on Climate Change (IPCC), Geneva, Switzerland. Please access report for extended list of writing team, editors, scientific steering committee and other contributing authors.
- [Luhman and Luhman, 2021] Luhman, E. and Luhman, T. (2021). Knowledge Distillation in Iterative Generative Models for Improved Sampling Speed. arXiv:2101.02388 [cs].

- [Pan et al., 2021] Pan, B., Anderson, G. J., Goncalves, A., Lucas, D. D., Bonfils, C. J., Lee, J., Tian, Y., and Ma, H.-Y. (2021). Learning to correct climate projection biases. *Journal of Advances in Modeling Earth Systems*, 13(10):e2021MS002509.
- [Rampal et al., 2022] Rampal, N., Gibson, P. B., Sood, A., Stuart, S., Fauchereau, N. C., Brandolino, C., Noll, B., and Meyers, T. (2022). High-resolution downscaling with interpretable deep learning: Rainfall extremes over new zealand. *Weather and Climate Extremes*, 38:100525.
- [Rombach et al., 2022] Rombach, R., Blattmann, A., Lorenz, D., Esser, P., and Ommer, B. (2022). High-resolution image synthesis with latent diffusion models. In *Proceedings of the IEEE/CVF conference on computer vision and pattern recognition*, pages 10684–10695.
- [Saharia et al., 2022a] Saharia, C., Chan, W., Chang, H., Lee, C., Ho, J., Salimans, T., Fleet, D., and Norouzi, M. (2022a). Palette: Image-to-image diffusion models. In *ACM SIGGRAPH 2022 Conference Proceedings*, pages 1–10.
- [Saharia et al., 2022b] Saharia, C., Chan, W., Saxena, S., Li, L., Whang, J., Denton, E. L., Ghasemipour, K., Gontijo Lopes, R., Karagol Ayan, B., Salimans, T., et al. (2022b). Photorealistic text-to-image diffusion models with deep language understanding. *Advances in neural information processing systems*, 35:36479–36494.
- [Saharia et al., 2022c] Saharia, C., Ho, J., Chan, W., Salimans, T., Fleet, D. J., and Norouzi, M. (2022c). Image super-resolution via iterative refinement. *IEEE Transactions on Pattern Analysis and Machine Intelligence*, 45(4):4713–4726.
- [Tong et al., 2021] Tong, Y., Gao, X., Han, Z., Xu, Y., Xu, Y., and Giorgi, F. (2021). Bias correction of temperature and precipitation over china for rcm simulations using the qm and qdm methods. *Climate Dynamics*, 57:1425–1443.
- [Vandal et al., 2017] Vandal, T., Kodra, E., Ganguly, S., Michaelis, A., Nemani, R., and Ganguly, A. R. (2017). Deepsd: Generating high resolution climate change projections through single image super-resolution. In *Proceedings of the 23rd acm sigkdd international conference on knowledge discovery and data mining*, pages 1663–1672.
- [Wan et al., 2024] Wan, Z. Y., Baptista, R., Boral, A., Chen, Y.-F., Anderson, J., Sha, F., and Zepeda-Núñez, L. (2024). Debias coarsely, sample conditionally: Statistical downscaling through optimal transport and probabilistic diffusion models. *Advances in Neural Information Processing Systems*, 36.
- [Wang et al., 2004] Wang, Z., Bovik, A. C., Sheikh, H. R., and Simoncelli, E. P. (2004). Image quality assessment: from error visibility to structural similarity. *IEEE transactions on image processing*, 13(4):600–612.
- [Zelinka et al., 2020] Zelinka, M. D., Myers, T. A., McCoy, D. T., Po-Chedley, S., Caldwell, P. M., Ceppi, P., Klein, S. A., and Taylor, K. E. (2020). Causes of higher climate sensitivity in cmip6 models. *Geophysical Research Letters*, 47(1):e2019GL085782.
- [Zhu et al., 2017] Zhu, J.-Y., Park, T., Isola, P., and Efros, A. A. (2017). Unpaired image-to-image translation using cycle-consistent adversarial networks. In *Proceedings of the IEEE International Conference on Computer Vision (ICCV)*.

Supplementary Information for “Conditional diffusion models for downscaling & bias correction of Earth system model precipitation”

*

Michael Aich^{1,2*}, Philipp Hess^{1,2}, Baoxiang Pan³,
Sebastian Bathiany^{1,2}, Yu Huang¹, Niklas Boers^{1,2,4}

¹Technical University Munich, Munich, Germany; School of Engineering & Design,
Earth System Modelling.

²Potsdam Institute for Climate Impact Research, Potsdam, Germany.

³Institute of Atmospheric Physics, Chinese Academy of Sciences, Beijing, China.

⁴Global Systems Institute and Department of Mathematics, University of Exeter,
Exeter, UK.

*Corresponding author. E-mail: michael.aich@tum.de;

1 Diffusion Models

1.1 Unconditional Diffusion Models

Diffusion Models can be separated into two parts, a forward and a backward diffusion process. The forward diffusion process is a probabilistic model $q(\mathbf{x}_t|\mathbf{x}_{t-1})$ that produces a noisy version of a given image \mathbf{x}_t in t noising steps. The model is chosen to be a Gaussian Model: $q(\mathbf{x}_t|\mathbf{x}_{t-1}) = \mathcal{N}(\mu(\mathbf{x}_{t-1}), \beta_t \mathbf{I})$, where β_t controls the amount of noise that is added in each step. In other studies, the model is often chosen to be of the form $q(\mathbf{x}_t|\mathbf{x}_{t-1}) = \mathcal{N}(\sqrt{1 - \beta_t} \mathbf{x}_{t-1}, \beta_t \mathbf{I})$ [Ho et al., 2020]. In practice, we use the reparametrization trick to sample from a Gaussian distribution by $\mathcal{N}(\mu, \sigma) = \mu + \sigma \epsilon$ where $\epsilon \sim \mathcal{N}(0, 1)$. A noisy version of \mathbf{x}_0 can thus be obtained as $\mathbf{x}_t = \sqrt{1 - \beta_t} \mathbf{x}_{t-1} + \beta_t \epsilon$ after t noising steps. The so-called noise scheduler β_t is chosen to add small amounts of noise in the beginning and larger amounts later on, in order to preserve a reasonable amount of information throughout the process.

The backward process $q(\mathbf{x}_{t-1}|\mathbf{x}_t)$ models how to restore the previous version $q(\mathbf{x}_{t-1})$ of a given image \mathbf{x}_t at a certain noise step t . This process is also modelled by a Gaussian $q(\mathbf{x}_{t-1}|\mathbf{x}_t) = \mathcal{N}(\mu(\mathbf{x}_t), \sigma(\mathbf{x}_t))$. The problem is that $\mu(\mathbf{x}_t)$ is not known. Using Bayes formula, the model can be rewritten as a product of Gaussians: $q(\mathbf{x}_{t-1}|\mathbf{x}_t) = \frac{q(\mathbf{x}_t|\mathbf{x}_{t-1})q(\mathbf{x}_{t-1})}{q(\mathbf{x}_t)}$. Each term is a Gaussian distribution and their product is also a Gaussian distribution. Computing the product and taking the mean of that expression is a valid way to model the backward process. In practice however, the distribution $q(\mathbf{x}_{t-1})$ is unknown, so we cannot explicitly compute $q(\mathbf{x}_{t-1}|\mathbf{x}_t)$. Predicting the state before a noising operation \mathbf{x}_{t-1} can be done by conditioning on the noisy image \mathbf{x}_t and the noise free image \mathbf{x}_0

$$q(\mathbf{x}_{t-1}|\mathbf{x}_t, \mathbf{x}_0) = \frac{q(\mathbf{x}_t|\mathbf{x}_{t-1}, \mathbf{x}_0)q(\mathbf{x}_{t-1}|\mathbf{x}_0)}{q(\mathbf{x}_t|\mathbf{x}_0)} \quad (1)$$

The terms on the right-hand side are Gaussians and can be explicitly computed. The resulting Gaussian has a mean term that depends on \mathbf{x}_t and \mathbf{x}_0 , while the variance is a constant depending on the timestep t .

$$q(\mathbf{x}_{t-1} | \mathbf{x}_t, \mathbf{x}_0) = \mathcal{N}(\mathbf{x}_{t-1}; \tilde{\boldsymbol{\mu}}(\mathbf{x}_t, \mathbf{x}_0), \sigma_t^2 \mathbf{I}) \quad (2)$$

$$\sigma_t^2 = \frac{1 - \bar{\alpha}_{t-1}}{1 - \bar{\alpha}_t} \cdot \beta_t \quad (3)$$

$$\tilde{\boldsymbol{\mu}}(\mathbf{x}_t, \mathbf{x}_0) = \frac{\sqrt{\bar{\alpha}_{t-1}}\beta_t}{1 - \bar{\alpha}_t} \mathbf{x}_0 + \frac{\sqrt{\bar{\alpha}_t}(1 - \bar{\alpha}_{t-1})}{1 - \bar{\alpha}_t} \mathbf{x}_t \quad (4)$$

with $\alpha_t = 1 - \beta_t$, $\bar{\alpha}_t = \prod_{s=0}^t \alpha_s$.

The following equation describes how \mathbf{x}_0 is connected to \mathbf{x}_t , when applying the forward diffusion model T times:

$$\begin{aligned} \mathbf{x}_t &= \sqrt{1 - \beta_t} \mathbf{x}_{t-1} + \sqrt{\beta_t} \boldsymbol{\epsilon}_{t-1} \\ &= \sqrt{\bar{\alpha}_t} \mathbf{x}_{t-2} + \sqrt{1 - \bar{\alpha}_t} \boldsymbol{\epsilon}_{t-2} \\ &= \dots \\ &= \sqrt{\bar{\alpha}_t} \mathbf{x}_0 + \sqrt{1 - \bar{\alpha}_t} \boldsymbol{\epsilon} \end{aligned} \quad (5)$$

where $\boldsymbol{\epsilon}, \dots, \boldsymbol{\epsilon}_{t-2}, \boldsymbol{\epsilon}_{t-1} \sim \mathcal{N}(\mathbf{0}, \mathbf{I})$. Solving for \mathbf{x}_0 yields:

$$\mathbf{x}_0 = \frac{1}{\sqrt{\bar{\alpha}_t}} (\mathbf{x}_t - \sqrt{1 - \bar{\alpha}_t} \boldsymbol{\epsilon}). \quad (6)$$

Combining Eq. 6 with Eq. 4 leads to:

$$\tilde{\boldsymbol{\mu}}(\mathbf{x}_t) = \frac{1}{\sqrt{\bar{\alpha}_t}} \left(\mathbf{x}_t - \frac{\beta_t}{\sqrt{1 - \bar{\alpha}_t}} \boldsymbol{\epsilon} \right).$$

The backward process (Eq. 2) is then modelled as:

$$q(\mathbf{x}_{t-1}|\mathbf{x}_t) = \mathcal{N}\left(\frac{1}{\sqrt{\alpha_t}}\left(\mathbf{x}_t - \frac{\beta_t}{\sqrt{\bar{\alpha}_t}}\epsilon\right), \sigma_t^2\mathbf{I}\right), \quad (7)$$

so given a noisy image in step t , this model will tell us how the less noisy version of that image \mathbf{x}_{t-1} looks like. The only unknown in this equation is ϵ . The idea is to parameterize ϵ with a neural network ϵ_θ . The objective of the network is then basically to estimate the noise that was added to a (noisy) image \mathbf{x}_{t-1} at each time step t :

$$\tilde{\boldsymbol{\mu}}_\theta(\mathbf{x}_t, t) = \frac{1}{\sqrt{\alpha_t}}\left(\mathbf{x}_t - \frac{\beta_t}{\sqrt{1-\bar{\alpha}_t}}\epsilon_\theta(\mathbf{x}_t, t)\right) \quad (8)$$

Using the reparametrization trick and inserting equation (Eq. 8) into equation (Eq. 2), the backward diffusion process (also called de-noising process) denotes as:

$$q(\mathbf{x}_{t-1}|\mathbf{x}_t) = \mathcal{N}\left(\frac{1}{\sqrt{\alpha_t}}\left(\mathbf{x}_t - \frac{\beta_t}{\sqrt{1-\bar{\alpha}_t}}\epsilon_\theta(\mathbf{x}_t, t)\right), \sigma_t^2\mathbf{I}\right). \quad (9)$$

Following the reparametrization trick, every iteration of the backward process takes the form:

$$\mathbf{x}_{t-1} \leftarrow \frac{1}{\sqrt{\alpha_t}}\left(\mathbf{x}_t - \frac{\beta_t}{\sqrt{1-\bar{\alpha}_t}}\epsilon_\theta(\mathbf{x}_t, t)\right) + \sigma_t\boldsymbol{\epsilon}_t \quad (10)$$

with $\boldsymbol{\epsilon}_t \sim \mathcal{N}(\mathbf{0}, \mathbf{I})$.

The neural network in the backward diffusion process can be learned through the following algorithm proposed by [Ho et al., 2020]:

Algorithm 1: Training

- 1 : **repeat**
- 2 : $\mathbf{x}_0 \sim q(\mathbf{x}_0)$
- 3 : $t \sim \text{Uniform}(\{1, \dots, T\})$
- 4 : $\boldsymbol{\epsilon} \sim \mathcal{N}(\mathbf{0}, \mathbf{I})$
- 5 : Take gradient descent step on
 $\nabla_\theta \|\boldsymbol{\epsilon} - \boldsymbol{\epsilon}_\theta(\sqrt{\bar{\alpha}_t}\mathbf{x}_0 + \sqrt{1-\bar{\alpha}_t}\boldsymbol{\epsilon}, t)\|^2$
- 6 : **until** converged

Model inference can be achieved with the following algorithm [Ho et al., 2020]:

Algorithm 2: Sampling

- 1 : $\mathbf{x}_T \sim \mathcal{N}(\mathbf{0}, \mathbf{I})$
- 2 : **for** $t = T, \dots, 1$ **do**
- 3 : $\mathbf{z} \sim \mathcal{N}(\mathbf{0}, \mathbf{I})$ if $t > 1$, else $\mathbf{z} = \mathbf{0}$
- 4 : $\mathbf{x}_{t-1} = \frac{1}{\sqrt{\alpha_t}}\left(\mathbf{x}_t - \frac{1-\alpha_t}{\sqrt{1-\bar{\alpha}_t}}\epsilon_\theta(\mathbf{x}_t, t)\right) + \sigma_t\mathbf{z}$
- 5 : **end for**
- 6 : **return** \mathbf{x}_0

The inference corresponds to generating a noise-free image, given a noisy input image.

1.1.1 Conditional Diffusion Models

The goal of a conditional diffusion model is to learn an approximation of the distribution $p(\mathbf{x}|c)$, where c is some conditional information. The method learns to model the reverse diffusion process as $p_\theta(\mathbf{x}_{t-1}|\mathbf{x}_t, c)$. Starting with a pure noisy image, it gets denoised in T steps. The forward diffusion process is identical to the unconditional case. The difference to the unconditional case is that the model has knowledge about the condition during the backward process. Theoretically, the model could also be conditioned during the forward process. The backward process looks as follows:

$$\mathbf{x}_{t-1} \leftarrow \frac{1}{\sqrt{\alpha_t}} \left(\mathbf{x}_t - \frac{\beta_t}{\sqrt{1 - \bar{\alpha}_t}} \epsilon_\theta(\mathbf{x}_t, c, t) \right) + \sigma_t \epsilon_t. \quad (11)$$

The condition is integrated by concatenating the condition and the noisy image in the color channel of the images. The network takes a two-channel image as input and produces a one-channel image as output in each backward step.

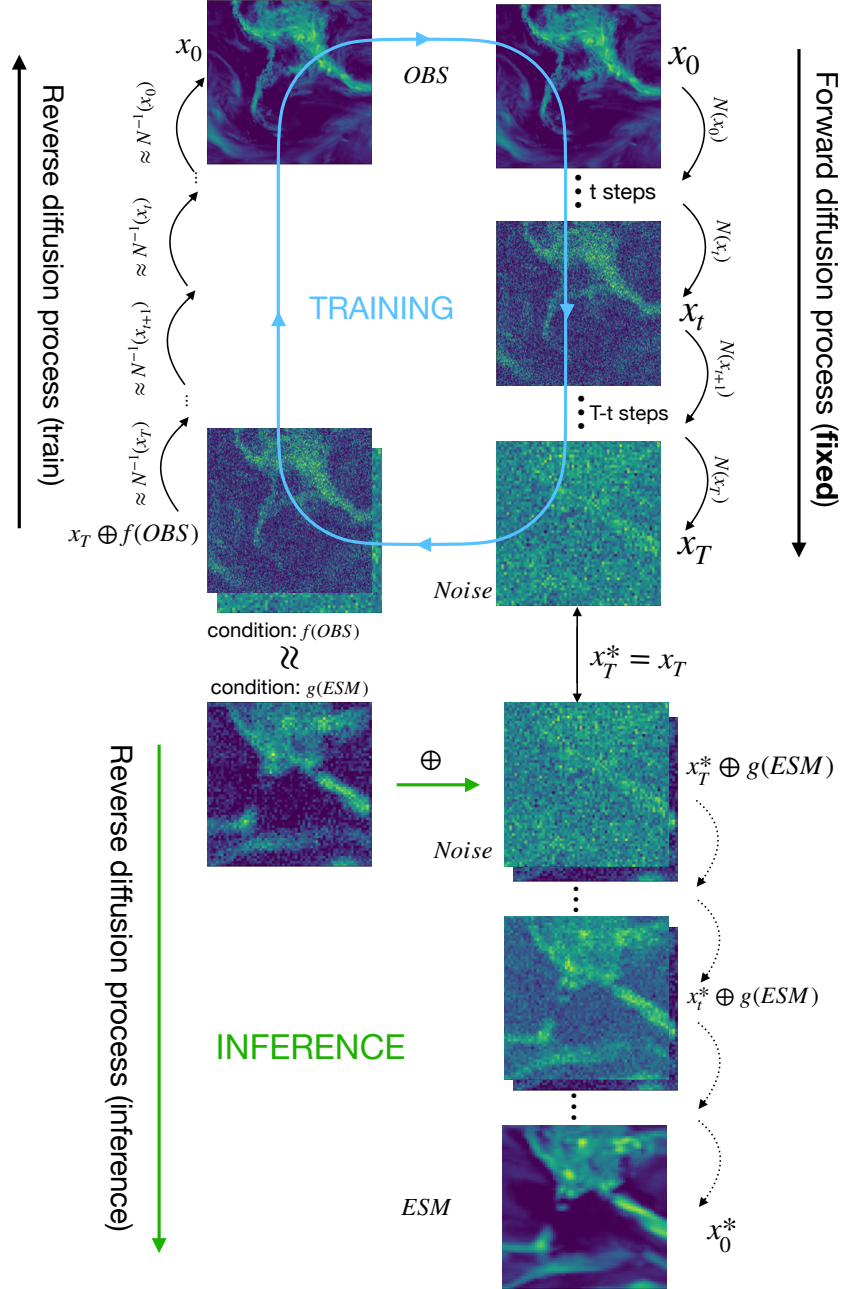


Fig. S1 Detailed visualisation of the training (blue) and inference process (green) of the conditional diffusion model introduced in our study. During the forward process (top to center), Gaussian noise $N(x_t)$ is added to an input image x_0 over t steps, following Eq.5, until x_t contains just noise. During the backward process (center to bottom) we concatenate a conditional image $f(OBS)$ with the noisy image x_t and train a neural network to remove the noise. The inference process uses the trained model. We also concatenate a purely noisy image x_t^* with the condition $g(ESM)$ and remove the noise from x_t^* with our trained model. The resulting image x_0^* follows the same distribution as x_0 , indicating that the bias correction and downscaling is achieved. The arrows between the training and inference part indicate that the image distribution at which the training ends is the same as the distribution the inference starts with.

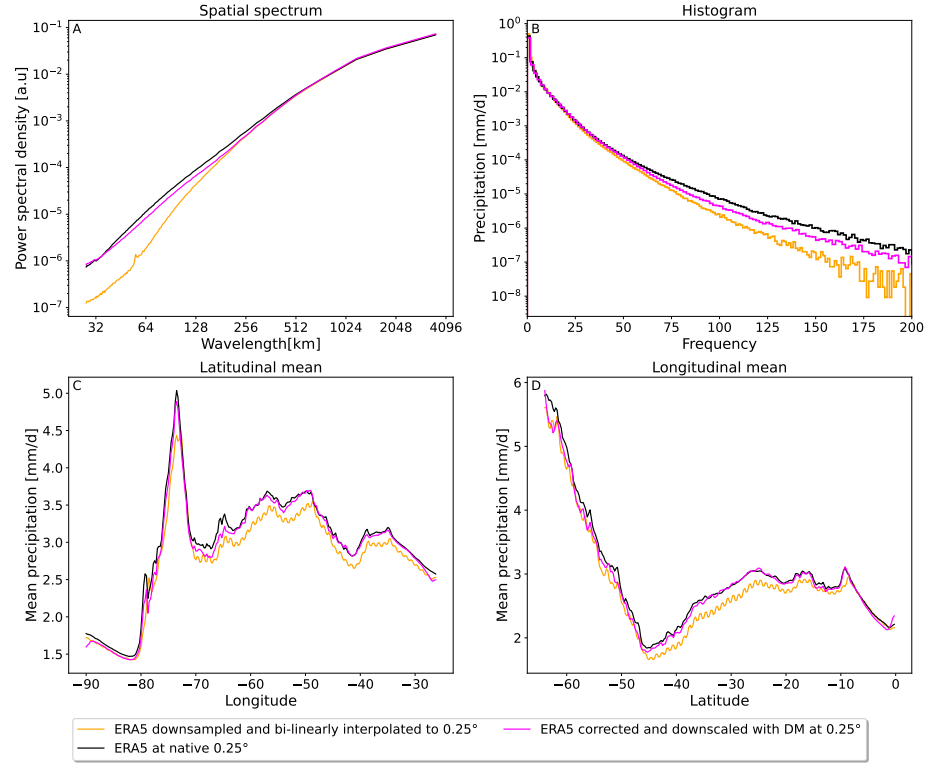


Fig. S2 Evaluation of the diffusion models performance to reconstruct ERA5 at 0.25° resolution from the embedded ERA5 data, obtained by downsampling to 1° via choosing only every fourth grid cell, and then bi-linearly interpolating back to 0.25°. In this case, the embedded ERA5 data mimics the ESM data in order to train the diffusion model (see Methods and main text). **(A)** Mean spatial power spectral densities (PSDs). **(B)** Histogram indicating the precipitation frequencies. **(C)** Latitude profile, given by the averaged longitudes over the validation period. **(D)** Longitude profile, given by the averaged latitudes over the validation period. Our diffusion model approximates the latitude and longitude profile of the original ERA5 reference data extremely well. The histogram shows also shows large improvements with slight deviations from the HR ERA5 reference data for extreme precipitation. The diffusion model manages to correct the small-scale spatial details and follows the target distribution closely.

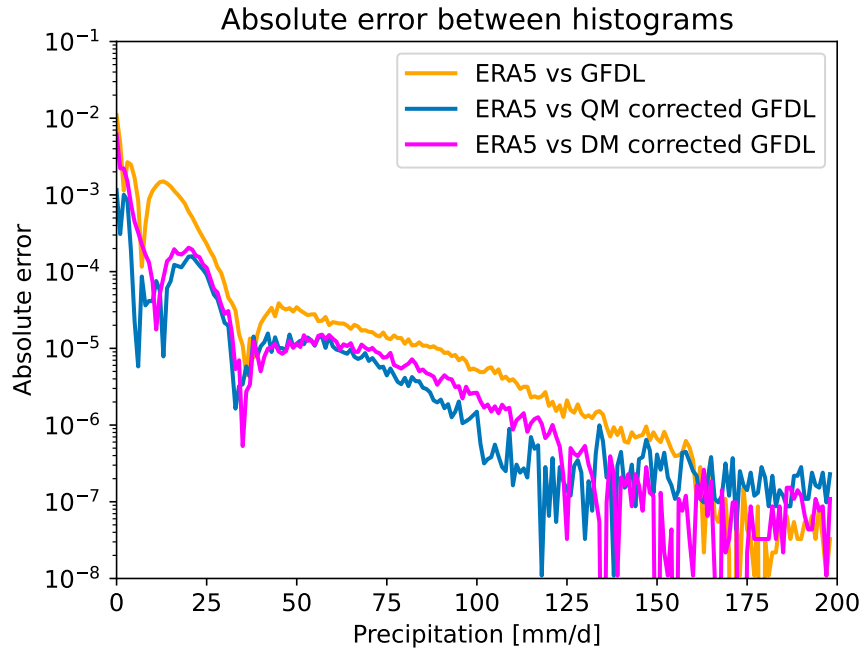


Fig. S3 The absolute error of the histograms between the high resolution ERA5 data (0.25°) and GFDL (bi-linearly upsampled to 0.25°) (orange), ERA5 and DM-corrected GFDL (magenta) and ERA5 and QM-corrected GFDL data (blue). The dips around 10 mm/d and 40 mm/d correspond to points where the histograms of ERA5 and its comparisons intersect. For very large precipitation values, our diffusion model outperforms the QM baseline, while it has slightly larger absolute error for smaller precipitation values.

References

- [Ho et al., 2020] Ho, J., Jain, A., and Abbeel, P. (2020). Denoising diffusion probabilistic models. *Advances in neural information processing systems*, 33:6840–6851.